Synthesis, Symmetry, and Physical Properties of Cerium Pyrophosphate

K. M. White,[†] P. L. Lee,[‡] P. J. Chupas,[‡] K. W. Chapman,[‡] E. A. Payzant,[§] A. C. Jupe,[†] W. A. Bassett,[||] C.-S. Zha,[⊥] and A. P. Wilkinson*,[†]

School of Chemistry and Biochemistry, Georgia Institute of Technology, Atlanta, Georgia 30332-0400, XOR, Advanced Photon Source, Argonne National Laboratory, Argonne, Illinois 60439, Materials Science and Technology Division, Oak Ridge National Laboratory, Oak Ridge, Tennessee 37831-6064, Geological Sciences, Department of Earth & Atmospheric Sciences, Snee Hall, Cornell University, Ithaca, New York 14853-1504, and CHESS, Wilson Lab, Cornell University, Ithaca, New York 14853

Received August 17, 2007. Revised Manuscript Received March 4, 2008

CeP_2O_7, a close structural relative of ZrP_2O_7, and many other $M^{IV}X_2O_7$ (X – P, V, As) phases, forms on heating $Ce(HPO_4)_2 \cdot xH_2O$ between ~300 and 600 °C and decomposes by oxygen loss at higher temperatures. In-situ X-ray diffraction measurements showed, for some precursor batches, the formation of CeP_2O_7 in two distinct stages. At room temperature, CeP_2O_7 is pseudocubic, but probably triclinic, displaying positive thermal expansion below ~115 °C. Above this temperature, there is a transition to cubic symmetry ($Pa\bar{3}$) with the linear coefficient of thermal expansion going to zero at ~450 °C and becoming negative at higher temperatures. CeP_2O_7 probably undergoes two phase transitions on compression below ~10.5 GPa. The phase existing between 0.65 and ~5 GPa is soft with an average bulk modulus of ~18 GPa.

Introduction

Cerium pyrophosphate belongs to a large family of $A^{IV}X_2O_7$ (A^{IV} = Si, Zr, Ce, Pb, Th, U, Pu, Ge, Hf; X^V = P, V, or As)[1–7] that have received recent attention due to a combination of the complex structures that are, in some cases, seen at low temperature and negative thermal expansion at high temperatures for some compositions.

The structures of these materials are related to that of NaCl, with a face centered arrangement of MO_6 octahedra sharing corners with P_2O_7 units. ZrP_2O_7 is probably the best studied member of this family. At high temperature (>290 °C), its crystal structure can be modeled in the cubic space group $Pa\bar{3}$ with linear P−O−P links.[8] At low temperatures, the material adopts a 3 × 3 × 3 superlattice,[8] and is now thought to be orthorhombic with P−O−P bonds bent away from 180°.[9,10] There is evidence for an incommensurate structure at slightly less than 290 °C.[11] SiP_2O_7,[12] TiP_2O_7,[13,14] SnP_2O_7,[15] and γ-GeP_2O_7[16] have also been reported to display superlattices at room temperature. TiP_2O_7 and SiP_2O_7 were reported to be cubic at room temperature, SnP_2O_7 was reported to be quasi-cubic[15] possibly monoclinic,[17] and γ-GeP_2O_7 is monoclinic, space group $P2_1/c$ or lower.[16]

CeP_2O_7 has never been well characterized, presumably in part due to its limited high temperature stability. Alberti et al. reported its synthesis by the dehydration of $Ce(HPO_4)_2 \cdot 1.33H_2O$ on heating to 600 °C.[18] Above 700 °C, it decomposes to give CeP_3O_9 and $CePO_4$.[19] Botto et al. reported a simple cubic (no supercell) structure for CeP_2O_7,[19] but Vollenkle et al. reported that at room temperature it had a 3 × 3 × 3 cubic superlattice also in space group $Pa\bar{3}$.[1]

In the current Article, we report an in situ X-ray dehydration study of $Ce(HPO_4)_2 \cdot xH_2O$ complemented by TGA measurements, high-resolution synchrotron powder diffraction measurements on CeP_2O_7, a thermal expansion study

* Corresponding author. E-mail: angus.wilkinson@chemistry.gatech.edu.
[†] Georgia Institute of Technology.
[‡] Argonne National Laboratory.
[§] Oak Ridge National Laboratory.
[||] Department of Earth & Atmospheric Sciences, Cornell University.
[⊥] CHESS, Cornell University.

(1) Vollenkle, H.; Wittmann, A.; Nowotny, H. *Monatsh. Chem.* **1963**, *94*, 956–963.
(2) Craig, D. F.; Hummel, F. A. *J. Am. Ceram. Soc.* **1972**, *55*, 532.
(3) Onken, H. *Naturwissenschaften* **1965**, *52*, 344.
(4) Karyakin, N. V.; Ghernorukov, G. N.; Bondareva, A. S. *Russ. J. Inorg. Chem.* **2001**, *46*, 701–704.
(5) Bjorklund, C. W. *J. Am. Chem. Soc.* **1958**, *79*, 6347–6350.
(6) Burdese, A.; Lucco Borlera, M. *Ann. Chim. (Rome)* **1963**, *53*, 333–343.
(7) Laud, K.; Hummel, F. A. *J. Am. Ceram. Soc.* **1971**, *54*, 296–298.
(8) Khosrovani, N.; Korthuis, V.; Sleight, A. W.; Vogt, T. *Inorg. Chem.* **1996**, *35*, 485–489.
(9) Birkedal, H.; Krogh Andersen, A. M.; Arakcheeva, A.; Chapuis, G.; Norby, P.; Pattison, P. *Inorg. Chem.* **2006**, *45*, 4346–4351.
(10) Stinton, G. W.; Hampson, M. R.; Evans, J. S. O. *Inorg. Chem.* **2006**, *45*, 4352–4358.
(11) Withers, R. L.; Tabira, Y.; Evans, J. S. O.; King, I. J.; Sleight, A. W. *J. Solid State Chem.* **2001**, *157*, 186–192.
(12) Tillmans, E.; Gebert, W.; Baur, W. H. *J. Solid State Chem.* **1973**, *7*, 69–84.
(13) Sanz, J.; Iglesias, J. E.; Soria, J.; Losilla, E. R.; Aranda, M. A. G.; Bruque, S. *Chem. Mater.* **1997**, *9*, 996–1003.
(14) Norberg, S. T.; Svensson, G.; Albertsson, J. *Acta Crystallogr., Sect. C* **2001**, *57*, 225–227.
(15) Gover, R. K. B.; Withers, N. D.; Allen, S.; Withers, R. L.; Evans, J. S. O. *J. Solid State Chem.* **2002**, *166*, 42–48.
(16) Losilla, E. R.; Cabeza, A.; Bruque, S.; Aranda, M. A. G.; Sanz, J.; Iglesias, J. E.; Alonso, J. A. *J. Solid State Chem.* **2001**, *156*, 213–219.
(17) Fayon, F.; King, I. J.; Harris, R. K.; Gover, R. K. B.; Evans, J. S. O.; Massiot, D. *Chem. Mater.* **2003**, *15*, 2234–2239.
(18) Alberti, G.; Costantino, U.; Zsinka, L. *Inorg. Nucl. Chem.* **1972**, *34*, 3549–3560.
(19) Botto, V. I. L.; Baran, E. J. *Z. Anorg. Allg. Chem.* **1977**, *430*, 283–288.

10.1021/cm702338h CCC: $40.75 © 2008 American Chemical Society
Published on Web 05/08/2008

of CeP_2O_7 using X-ray diffraction, and high-pressure powder diffraction measurements. The results are compared to those for other $A^{IV}X^{V}{}_2O_7$ compounds.

Experimental Section

Synthesis. Cerium pyrophosphate was synthesized using the method reported by Alberti et al.[18] Cerium(IV) sulfate hydrate powder was added to 10 M H_3PO_4 (P:Ce molar ratio of 15:1) while stirring under reflux. A precipitate formed after a few minutes. The temperature was reduced slightly, and the mixture was heated for a further ~100 h with occasional stirring. The precipitate was recovered by filtration, washed, and then air-dried. This precursor ($Ce(HPO_4)_2 \cdot xH_2O$) was stored over a saturated solution of NaCl in a desiccator. An off-white sample of CeP_2O_7 was obtained by first heating the precursors at 200 °C for 20 h, then 400 °C for 4 h, and finally at 600 °C for 16 h.

Thermal Analysis. TG/DTA analyses were performed on $Ce(HPO_4)_2 \cdot xH_2O$, using a Seiko SSC/5200 TG/DTA 3200 instrument, under flowing nitrogen with a ramp rate of 5 °C/min from room temperature to 1000 °C.

In-Situ Synchrotron Diffraction Measurements of CeP_2O_7 Formation and Decomposition. The dehydration of $Ce(HPO_4)_2 \cdot xH_2O$ was followed in real time by X-ray powder diffraction using a capillary sample in a furnace[20] with argon gas flowing through the sample. For the data presented, a ramp rate of 4 °C/min was used, closely matching that used for the TGA experiment (5 °C/min) on the same sample. The diffraction measurements were conducted at the Advanced Photon Source, Argonne National Laboratory, beam line 11-ID-B, using X-rays from an elliptical multipole wiggler,[21] monochromated by a horizontally scattering mosaic silicon Laue crystal[22] ($\lambda = 0.1376$ Å) and a MAR 345 image plate detector.

Laboratory X-ray Powder Diffraction Measurements. Ambient temperature data were recorded for the precursor and CeP_2O_7 using a Scintag diffractometer with a Cu tube and a Peltier-cooled solid state detector. High temperature measurements on CeP_2O_7 were performed using a Panalytical X'Pert Pro instrument, located in the High Temperature Materials Laboratory at Oak Ridge National Laboratory. A 0.04 rad soller slit, 10 mm mask, and programmable divergence slit (0.5°) were used on the incident beam side, while a 0.04 rad soller slit, nickel foil, and an X'Celerator position sensitive detector were used on the diffracted beam side. An Anton Paar XRK 900 furnace was used to heat the sample in air. On the basis of previous measurements, the temperature calibration for this furnace is believed to be reliable. Data were collected over the angular range 13−140° 2θ.

High-Resolution Synchrotron X-ray Diffraction Measurements. High-resolution powder diffraction patterns were recorded for CeP_2O_7 at the Advanced Photon Source. An initial room temperature high-resolution pattern was collected at beam line 32-ID. This experiment used $\lambda = 0.4961$ Å X-rays from an undulator and a double crystal diamond (111) monochromator. The diffractometer employed a triple axis geometry, with 11 scintillation detectors each with its own Si(111) analyzer crystal. Additionally, high-resolution powder patterns were collected at several temperatures on beam line 1-BM using a triple-axis arrangement with a single Si(111) analyzer crystal and a Cyberstar scintillation counter. A sagittally focusing Si(111) double-crystal monochromator and palladium-coated collimating and focusing mirrors were used to condition the beam.[23] A wavelength of 0.6051 Å was employed for these measurements. This beam line delivered slightly worse resolution than that seen at 32-ID. High temperature measurements (<800 °C) were made using a furnace designed by P. J. Chupas,[20] and low temperature measurements ($T \approx 14$ and 150 K) were made using a Displex closed cycle refrigerator. Capillary geometry (0.7 mm diameter thin wall silica glass) was used for the high temperature measurements, and a flat plate sample was used in the cryostat. Temperature was measured in the furnace using a thermocouple whose tip was in the capillary tube with the sample a short distance from the material examined with X-rays. The accuracy of these temperature measurements was not verified using a standard.

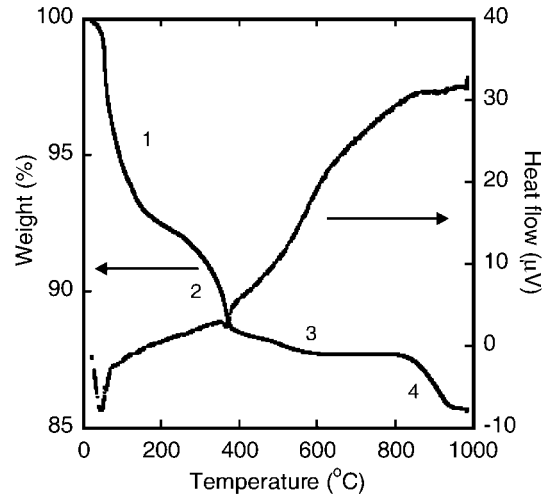

Figure 1. TG/DTA data for the precursor material $Ce(HPO_4)_2 \cdot xH_2O$ with a 5 °C/min ramp in nitrogen.

High-Pressure Powder Diffraction. Powder diffraction data were recorded up to ~10.5 GPa, for a sample of CeP_2O_7 in a DAC, designed by W. Bassett (Hydrothermal Diamond Anvil Cell),[24] using the CHESS facility at Cornell University. The diamonds were ~1.6 mm thick and had 0.6 mm cullet faces. The sample was contained within a 300 μm diameter hole in a 125 μm thick rhenium gasket. A methanol:ethanol pressure transmitting medium was used. An X-ray beam ($E = 25.10$ keV, $\lambda = 0.4940$ Å) from a double crystal Ge(111) monochromator collimated to ~50 μm was used along with a MAR 345 image plate detector. Pressure calibration was performed using the ruby fluorescence method. NaCl was used to calibrate the sample to detector distance and the detector tilt. FIT-2D[25] was used to integrate the image plate data.

Results

TGA/DTA and In-Situ X-ray Diffraction Study of CeP_2O_7 Formation and Decomposition. Alberti et al. have previously reported a TGA measurement for the dehydration of $Ce(HPO_4)_2 \cdot xH_2O$.[18] Here, we present TGA data (Figure 1) for our precursor along with complementary DTA and diffraction measurements. These data were all collected on

(20) Chupas, P. J.; Ciraolo, M. F.; Hanson, J. C.; Grey, C. P. *J. Am. Chem. Soc.* **2001**, *123*, 1694–1702.
(21) Beno, M. A.; Kurtz, C.; Munkholm, A.; Rutt, U.;.; Engbretson, M.; Jennings, G.; Linton, J.; Knapp, G. S.; Montano, P. A. *Nucl. Instrum. Methods Phys. Res., Sect. A* **2001**, *467−468*, 694–698.
(22) Rutt, U.; Beno, M. A.; Strempfer, J.; Jennings, G.; Kurtz, C.; Montano, P. A. *Nucl. Instrum. Methods Phys. Res., Sect. A* **2001**, *467−468*, 1026–1029.
(23) Lang, J. C.; Srajer, G.; Wang, J.; Lee, P. L. *Rev. Sci. Instrum.* **1999**, *70*, 4457–4462.
(24) Bassett, W. A.; Shen, A. H.; Bucknum, M.; Chou, I.-M. *Rev. Sci. Instrum.* **1993**, *64*, 2340.
(25) Hammersley, A. P.; Svensson, S. O.; Hanfland, M.; Fitch, A. N.; Hausermann, D. *High-Pressure Res.* **1996**, *14*, 235–248.

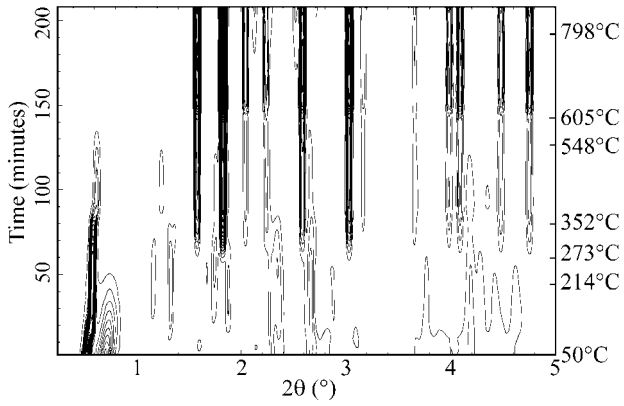

Figure 2. Contour plot showing synchrotron powder diffraction data collected in situ during the dehydration of $Ce(HPO_4)_2 \cdot 1.46H_2O$. The measurements were made using a capillary geometry under flowing argon with a ramp rate of ~4 °C/min.

the same batch of precursor material at similar, although not identical, heating rates and provide additional insight beyond the work of Alberti and co-workers.

There were four obvious regions of weight loss (marked on Figure 1). Assuming that between 600 and 800 °C the product was CeP_2O_7 (supported by X-ray studies), the starting precursor could be formulated as $Ce(HPO_4)_2 \cdot 1.46H_2O$. Below ~ 155 °C (region 1), ~1.40 H_2O per mole of Ce was lost. Dehydroxylation presumably occurred in regions 2 (~0.86 mol of H_2O per mol Ce) and 3 (~0.20 mol of H_2O). The sum of the weight losses in these regions (1.06 H_2O) is consistent with complete dehydroxylation of $Ce(HPO_4)_2$ given the uncertainty in deciding where the loss of water ends and dehydroxylation begins. It is not entirely clear why dehydroxylation occurs in two steps, although it seems likely that the precursor batch had some compositional, structural, or microstructural inhomogeneities. Our in-situ X-ray data (see next paragraph) and the observation that some batches of precursor prepared under slightly different conditions gave a smaller weight loss in region 3 support this hypothesis. Regions 1 and 2 were associated with endotherms, as expected for dehydration and dehydroxylation, although the endotherm for region 2 was not very pronounced. The weight loss between 800 and 1000 °C is attributable to oxygen loss of ~0.18 mol of O_2 per mol of CeP_2O_7 and is consistent with the reduction of Ce(IV) to give a mixture of $CePO_4$ and CeP_3O_9. These were the products seen after heating CeP_2O_7 to 725 °C for extended time periods and recovering them to room temperature.

To determine the nature and sequence of phases formed during dehydration, an in-situ powder diffraction study was performed on the precursor $Ce(HPO_4)_2 \cdot 1.46H_2O$ (see Figure 2). The precursor batch used for the TGA/DTA measurements was also employed for this in-situ diffraction study, but a slightly slower heating rate was used (4 °C/min). The laboratory powder X-ray data for the precursor, taken in flat plate Bragg−Brentano geometry, showed peaks fully consistent with the pattern for $Ce(HPO_4)_2 \cdot 1.33H_2O$ (33-0328) in the ICDD powder diffraction database. The first pattern in the data from the in-situ study using high energy X-rays at beam line 11-ID-B showed not only sharp features similar to the laboratory X-ray pattern for the sample, but also a relatively broad peak at 2θ ~0.7° ($d \approx 11$ Å) that may be a reflection from the main phase that did not show up well in the flat plate data due to preferred orientation in the platy precursor material. After the temperature ramp for the diffraction experiment started, the peaks at 2θ ~0.5° ($d \approx 16$ Å) and 0.7° ($d \approx 11$ Å) both shifted to the right, and by around 40 min into the ramp (~200 °C), the broader of the two peaks had disappeared. Along with these changes, some new Bragg peaks appear. All of the major peaks present at 50 min into the experiment are close to those in the ICDD powder diffraction pattern for $Ce(HPO_4)_2 \cdot 0.33H_2O$ (34-0466), although the precise hydration state can not be established from these X-ray data. These changes in the diffraction pattern were associated with the first major weight loss in the TGA data. On further heating and starting at ~275 °C, the intensity of the lowest angle diffraction peak decreased and a strong set of peaks attributable to CeP_2O_7 started to grow in, for example, the peak at 2θ ~2.6° ($d \approx 3.0$ Å). This first appearance of CeP_2O_7 was associated with the end of the second major weight loss in the TGA data. At around 350 °C, the lowest angle major diffraction peak appears to shift to higher angle. This peak does not disappear completely until ~580 °C, and this coincided with both the end of the third major weight loss in the TGA data and an increase in intensity of the CeP_2O_7 peaks, implying that this phase was ultimately transformed to more CeP_2O_7 and that it contained hydroxyl groups whose removal led to the weight loss. At around 800 °C, some new peaks started to appear in the diffraction data that were consistent with CeP_3O_9 and $CePO_4$ (monazite) forming as CeP_2O_7 decomposed. Oxygen loss was also seen in the TGA data with an onset at ~800 °C. The two-stage formation of CeP_2O_7 during the temperature ramp suggests that the precursor material was not completely homogeneous in either composition or, perhaps, microstructure, even though all of the diffraction peaks immediately prior to the first formation of CeP_2O_7 seem to be related to those previously reported for $Ce(HPO_4)_2 \cdot 0.33H_2O$ (34-0466).

Metric Symmetry and Unit Cell Size. Initial room-temperature powder diffraction measurements recorded on a laboratory diffractometer for CeP_2O_7 showed slight shoulders on some of the Bragg peaks, suggesting a symmetry lower than cubic. Subsequent high-resolution synchrotron powder diffraction measurements confirmed this. Peak positions obtained by fitting the synchrotron data using JADE[26] were used as input to the CRYSFIRE[27] indexing software. A triclinic cell, $a = 6.061$ Å, $b = 8.55$ Å, $c = 6.070$ Å, $\alpha = 90.16°$, $\beta = 90.15°$, $\gamma = 90.00°$, gave the highest figure of merit. This cell was transformed to give a pseudocubic cell ~8.57 Å on edge. A structure refinement was attempted in space group $P1$ using TOPAS[28] along with starting atom positions determined by applying all of the symmetry operations in space group $Pa\bar{3}$ to the atomic coordinates for the high temperature cubic ZrP_2O_7 structure. Initially, the coordinates were fixed and the lattice constants optimized

(26) *JADE, 6.5.22*; Materials Data, Inc.; Livermore, CA, 1995–2005.
(27) *CRYSFIRE Suite: R. Shirley, The CRYSFIRE System for Automatic Powder Indexing*, 2002.
(28) Coelho, A. A. *J. Appl. Crystallogr.* **2000**, *33*, 899–908.

by a simulated annealing-type procedure. The lattice constants were randomly selected within the ranges 8.54−8.60 Å and 89.5−90.5° and then refined to convergence. The process of perturbation and refinement was repeated many times. In the final stage of the analysis, an attempt was made to vary the atomic coordinates as well. The best fit resulted in: $a = 8.56851(4)$ Å, $b = 8.58546(8)$ Å, $c = 8.58265(7)$ Å; $\alpha = 89.9281(6)°$, $\beta = 89.9097(6)°$, $\gamma = 89.8273(5)°$ ($R_{wp} = 10.18\%$, $R_{Bragg} = 2.89\%$, GOF = 6.59). While the unit cell is triclinic, it is clearly pseudocubic. The quoted standard deviations on the lattice constants were obtained directly from the Rietveld least-squares fit and probably significantly underestimate the true uncertainty. This triclinic model accounted for all of the splittings in the major diffraction peaks, but the refined structural model was chemically/physically unrealistic and there were many very weak peaks that were unaccounted for, indicating impurities or a supercell. The weak peaks could not be assigned to likely impurities such as the known high temperature degradation products $CePO_4$ and CeP_3O_9, and there were no obvious low-angle weak peaks to indicate a supercell. Efforts to obtain high-quality electron diffraction patterns for CeP_2O_7 to confirm or refute the presence of a superlattice were unsuccessful as isolated single crystallites could not be found in the sample. As we did not determine a chemically plausible structural model by refinement, we present Rietveld fits to selected peaks in the 32ID data obtained using cubic ZrP_2O_7 coordinates without optimization and both triclinc and cubic lattice constants to illustrate the splittings that were observed in the raw data and the ability of a triclinic distortion from the simple cubic $Pa\bar{3}$ structure to account for them (Figure 3). We also analyzed the available room temperature, −123 °C (150 K), and −259 °C (14 K) synchrotron patterns collected at beam line 1-BM using a triclinic lattice along with an atomic model that was derived directly from the cubic $Pa\bar{3}$ structure of ZrP_2O_7, without any optimization of the atomic coordinates, to get estimates of the lattice constants at these temperatures. The lattice constants from these fits are presented in Table 1.

Variable-temperature high-resolution synchrotron powder diffraction data were recorded to look for phase transitions in CeP_2O_7. At most temperatures examined, data were only recorded in regions around 14 strong low-angle groups of peaks, but complete diffraction patterns were measured at room temperature and ∼300 °C. In Figure 4, we show changes in two of these groups of peaks as a function of temperature. The splittings/shoulders that were present at room temperature disappeared at ∼175 °C, and at high temperature the peaks moved to higher angle, indicating the onset of negative thermal expansion. Rietveld refinements using the full pattern recorded at ∼300 °C and a cubic ($Pa\bar{3}$) model, with either isotropic or anisotropic atomic displacement parameters, led to very high-quality fits, strongly suggesting that the high temperature phase is metrically cubic. See Figure 5 for the profile fit resulting from the isotropic refinement, and Table 2 for a summary of the refinement results. The low-temperature high-resolution powder diffraction data, recorded at −123 °C (150 K) and −259 °C (14 K), showed only small changes in the observed

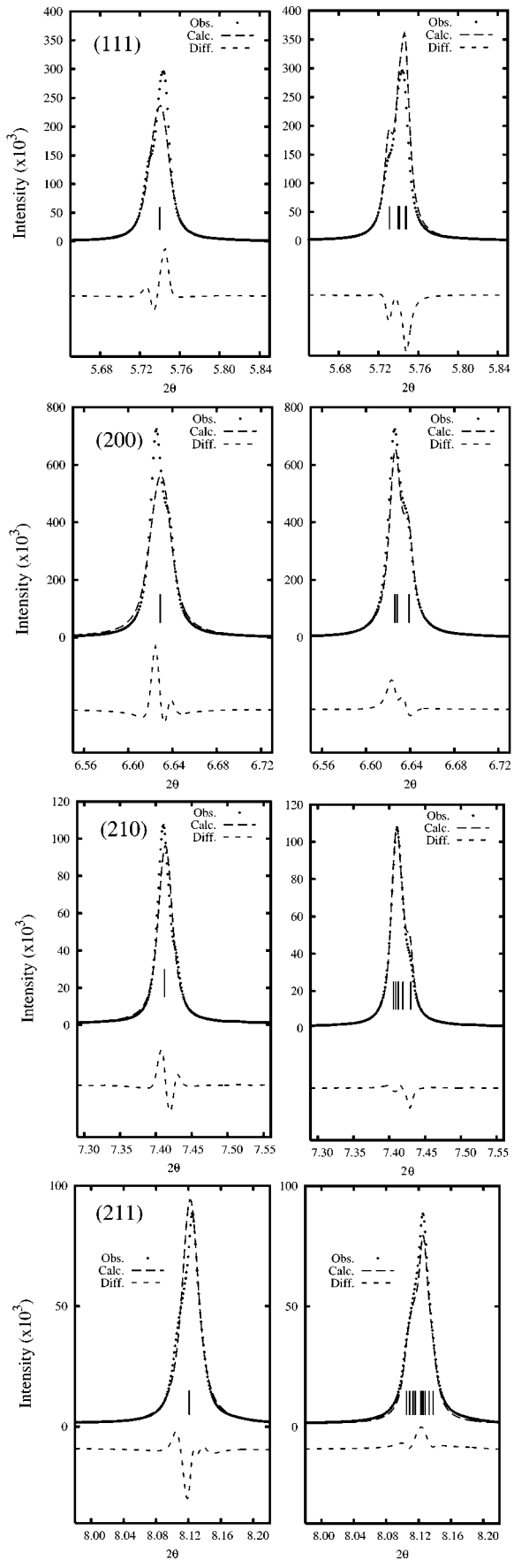

Figure 3. Comparison of fits with cubic (left) and triclinic (right) lattices to selected peaks in the high-resolution room-temperature powder X-ray diffraction pattern of CeP_2O_7. In each case, the atomic coordinates have been fixed at the values reported for cubic ZrP_2O_7. Panels on the left side give Miller indices for the cubic $Pa\bar{3}$ structure.

Table 1. Lattice Constants and Unit Cell Volume versus Temperature As Determined from Four Complete Synchrotron Powder Patterns Recorded on Beam Line 1-BM

	~300 °C	RT (~25 °C)	−123 °C	−259 °C
a/Å	8.59259(2)	8.5754(2)	8.5548(1)	8.5543(1)
b/Å	8.59259(2)	8.5933(2)	8.5756(1)	8.5763(1)
c/Å	8.59259(2)	8.5855(2)	8.5710(1)	8.5718(1)
α/deg	90	89.952(3)	89.917(1)	89.910(1)
β/deg	90	89.928(3)	89.884(1)	89.872(1)
γ/deg	90	89.825(2)	89.757(1)	89.742(1)
V/Å^3	634.41	632.67	628.78	628.85

peak splittings when compared to the room-temperature data, and there appeared to be almost no thermal contraction on cooling from −123 °C (150 K) to −259 °C (14 K), although there was significant thermal contraction between room temperature and −123 °C (150 K) (see Table 1).

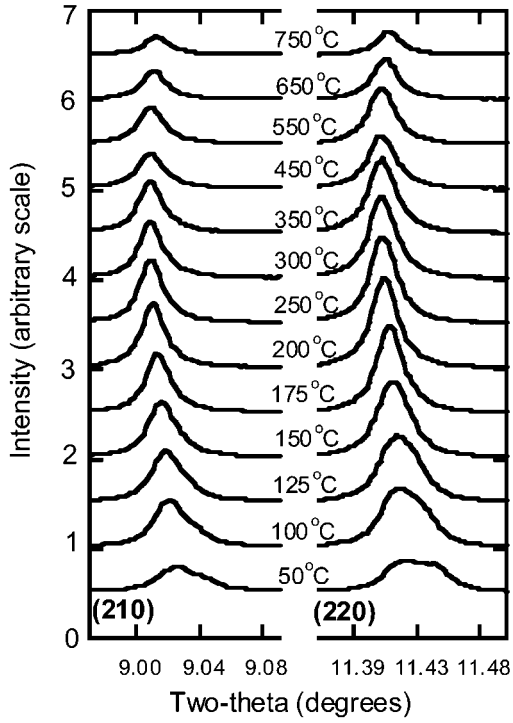

Figure 4. The cubic (210) and (220) peaks in the high-resolution diffraction data for CeP_2O_7 as a function of temperature (λ = 0.6051 Å). A phase transition is seen at ~175 °C, and there is negative thermal expansion at high temperature.

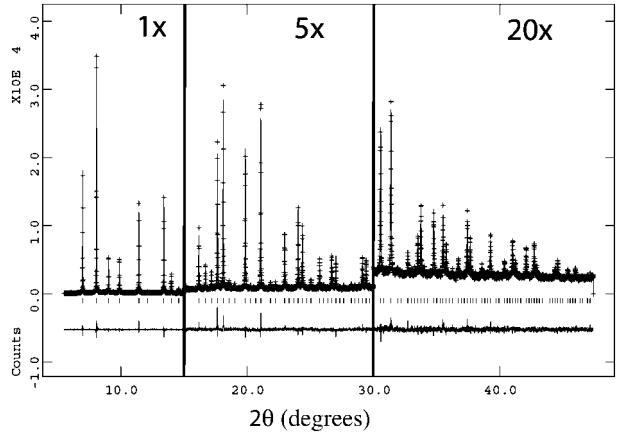

Figure 5. Rietveld fit to the 300 °C high-resolution X-ray diffraction data for CeP_2O_7 using a cubic $Pa\bar{3}$ model.

Table 2. Summary of Structure Refinement Results for CeP_2O_7 at ~300 °C[a]

wavelength/Å	0.6051
lattice constant *a*/Å	8.59259(2)
space group	$Pa\bar{3}$
ρ_x/g cm^{-3}	3.29
μ/cm^{-1}	47
absorption correction	yes

parameter	isotropic	anisotropic
Ce ($x = y =$ z)	0.000	0.0
Ce $U_{iso/equiv}$	0.0244(1)	0.025
Ce U_{11}; U_{12}		0.02544(9); 0.0002(3)
P ($x = y =$ z)	0.4000(1)	0.4002(1)
P $U_{iso/equiv}$	0.0311(5)	0.029
P U_{11}; U_{12}		0.0291(5); 0.0065(6)
O1 *x*	0.4448(3)	0.4449(3)
O1 *y*	0.2315(2)	0.2323(2)
O1 *z*	0.4324(3)	0.4294(4)
O1 $U_{iso/equiv}$	0.0827(1)	0.085
O1 U_{11}; U_{22}; U_{33}		0.089(3); 0.046(2); 0.120(3)
O1 U_{12}; U_{13}; U_{23}		0.025(2); 0.023(2); 0.028(2)
O2 ($x = y =$ z)	0.5000	0.5000
O2 $U_{iso/equiv}$	0.120(2)	0.13
O2 U_{11}; U_{12}		0.132(2); −0.042(4)
R_{wp}	7.89%	7.54%
R_F^2	5.4%	4.2%
χ^2	1.99	1.82
6 × Ce–O/Å	2.126(2)	2.140(2)
3 × P–O1/Å	1.524(2)	1.514(2)
1 × P–O2/Å	1.489(2)	1.485(2)

[a] Values from models with both isotropic and anisotropic atomic displacement parameters are included.

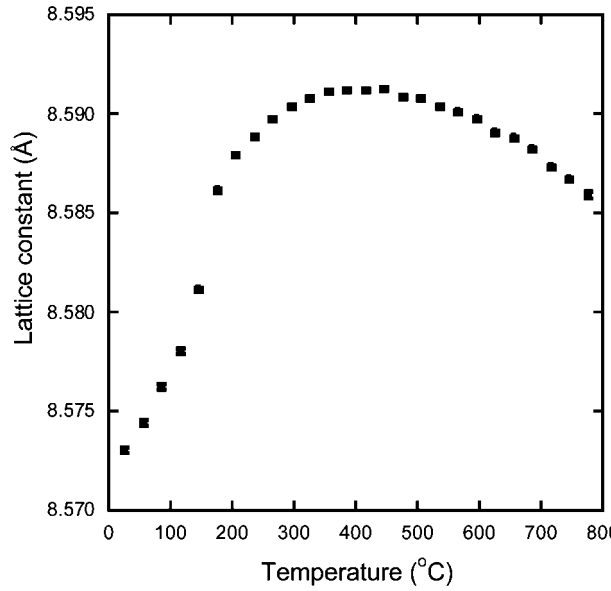

Figure 6. Pseudocubic/cubic lattice parameter versus temperature for CeP_2O_7.

Thermal Expansion of CeP_2O_7. High-temperature laboratory powder X-ray diffraction was used to examine the thermal expansion of CeP_2O_7 at up to 805 °C. During these measurements, Ce(III) phosphate decomposition products were observed at 775 and 805 °C. The pseudocubic and cubic lattice constants for CeP_2O_7, obtained from Rietveld fits to this data using GSAS and a cubic $Pa\bar{3}$ model, are shown in Figure 6 and are available as Supporting Information. These data suggest a phase transition between 115 and 175 °C, broadly consistent with the high-resolution synchrotron data. Between 25 and 115 °C, the effective linear CTE is 6.5 ×

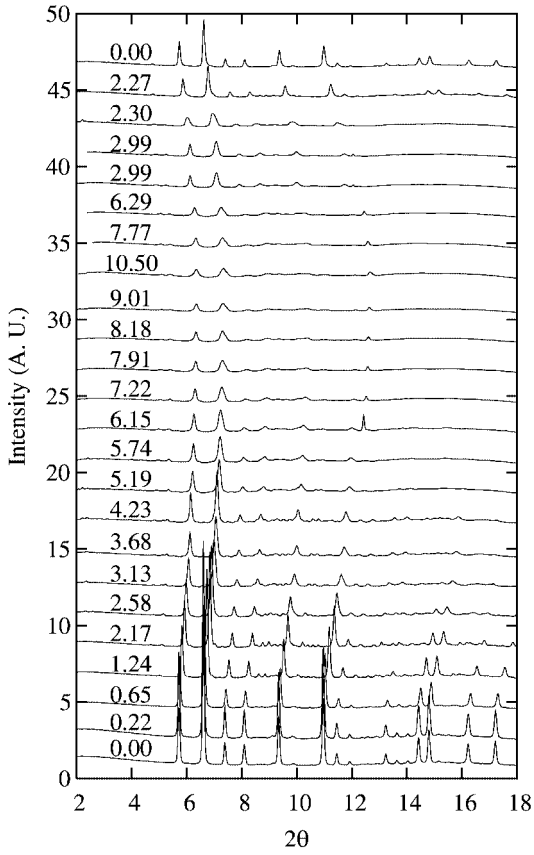

Figure 7. High-pressure powder diffraction data for CeP_2O_7 on compression and decompression ($\lambda = 0.4940$ Å). The sharp peak that first appears in the 6.15 GPa data set during compression is from the rhenium gasket, and not from the sample.

10^{-6} K^{-1}. The lattice constant shows a maximum at ~445 °C, and between 445 and 805 °C the linear CTE is -1.9×10^{-6} K^{-1}.

High-Pressure Diffraction Studies of CeP_2O_7. Powder diffraction patterns on compression and decompression are presented in Figure 7. Starting at around 0.65 GPa, some weak peaks at low angle and between 8° and 9° 2θ become apparent, suggesting a possible low-pressure phase transition. At higher pressures, the Bragg peaks broadened, but there were no sudden changes in the diffraction data for the CeP_2O_7 on compression up to the pressure limit of the experiment (~10.5 GPa). The sharp peak that first appears in the 6.15 GPa data at around 12° 2θ is from the rhenium gasket, not CeP_2O_7.

Initially, the diffraction data were fit to extract the full width at half-maximum (fwhm) of the first strong peak to look for indications of any phase transitions. Subsequently, the complete patterns were then fit to a cubic model using the LeBail method in TOPAS,[28] to extract a pseudocubic lattice constant as a function of pressure. As no splittings could be observed in any of the peaks at low pressure, the use of a lower symmetry model was not explored even though the high-resolution ambient pressure measurements clearly indicate a symmetry lower than cubic at room temperature. The fwhm for the first major peak showed no obvious jumps on compression that might be associated with a phase transition. However, an examination of unit cell volume versus pressure shows pronounced stiffening at around 5 GPa that is probably associated with a phase transition (see Figure 8). Compressibilities in the ranges 0−3.7 and 7−10.5 GPa were estimated to be $5.6(2) \times 10^{-2}$ and $5.6(6) \times 10^{-3}$ GPa^{-1}, respectively, by fitting straight lines to $\ln(V)$ versus P for the compression of CeP_2O_7 as shown in Figure 8; these values correspond to bulk moduli of ~18 and 180 GPa for the two phases.

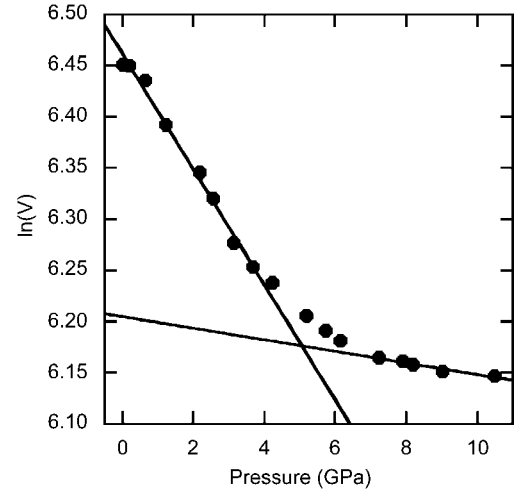

Figure 8. Unit cell volume versus pressure data for CeP_2O_7 indicate a phase transition at around 5 GPa, leading to a dramatic stiffening of the structure.

Discussion

The TGA/DTA and in-situ diffraction measurements examining the dehydration of $Ce(HPO_4)_2 \cdot xH_2O$ generally confirm the prior observations of Alberti et al.[18] However, we see for some batches of precursor a two-stage formation of CeP_2O_7, perhaps due to inhomogeneities in the precursor, with first formation of crystalline CeP_2O_7 at ~300 °C, a lower temperature than reported by Alberti et al., and complete conversion to the pyrophosphate by ~600 °C.

While most members of the $M^{IV}P_2O_7$ family were initially reported to have cubic symmetry, distortions away from the ideal cubic $Pa\bar{3}$ structure have been seen for γ-GeP_2O_7 (monoclinic at ambient temperature),[16] SnP_2O_7 (monoclinic by NMR at ambient temperature),[17] and ZrP_2O_7 (orthorhombic at ambient temperature).[9,10] Distortions away from cubic symmetry at low temperature, and the superlattices that have been reported, are presumably driven by a desire to avoid average P−O−P bond angles of 180°. Our experiments conclusively demonstrate that CeP_2O_7 also shows a small distortion away from cubic symmetry at room temperature and below. While a definitive unit cell determination for this material awaits further work, as we were unable to assign several weak peaks in our diffraction data or obtain a chemically plausible structure refinement, a triclinic cell related by transformation to $a = 8.56851(4)$ Å, $b = 8.58546(8)$ Å, $c = 8.58265(7)$ Å; $\alpha = 89.9281(6)°$, $\beta = 89.9097(6)°$, $\gamma = 89.8273(5)°$ seems likely. A triclinic subcell of this type has been previously reported for SnP_2O_7 in the temperature range 833−1103 °C (560−830 K).[15]

Both the laboratory X-ray and the synchrotron variable-temperature diffraction experiments indicate a phase transi-

tion in the temperature range 115−175 °C. Rietveld analysis of the synchrotron data collected at 300 °C demonstrates that the high temperature structure is very well described as cubic, $Pa\bar{3}$, $a = 8.59259(2)$ Å. Phase transitions to a simple cubic $Pa\bar{3}$ structure of this type have been reported for both ZrP_2O_7 and ZrV_2O_7.[29] On heating SnP_2O_7 from room temperature, two phase transitions have been observed, but this compound does not become cubic below 1323 °C.[15]

Our structure refinement for CeP_2O_7 at ∼300 °C, while fully consistent with cubic metric symmetry, is indicative of considerable structural disorder with large and highly anisotropic thermal parameters for both O1 and O2 (see Table 2). The anisotropy and magnitudes of the atomic displacement parameters (ADPs) for O2 (large displacements perpendicular to the P–P direction) are consistent with a local structure that has bent P−O−P links. However, the different PO_4 group orientations average to give apparently linear P−O−P links as is typical of ZrP_2O_7 and its relatives in their cubic forms.[8] The apparent P−O(–P) and P−O(–Ce) bond lengths are similar to one another, with the P−O(–P) distance being shorter, as seen in disordered high-temperature ZrP_2O_7.[8] However, in ordered orthorhombic ZrP_2O_7, the difference between the average P−O(–P) and P−O(–Zr) bond lengths is greater and the average P−O(–P) distance is longer than the average P−O(–Zr).[10] The apparently short P−O(–P) distance in CeP_2O_7 is probably associated with displacements of O2 away from the P−P vector bringing the pair of P atoms closer together. The estimated Ce−O bond length of 2.140(2) Å from our anisotropic refinement is unexpectedly short based on recently reported bond valence sum parameters for Ce(IV) coordinated to oxygen,[30] which suggest a bond length of 2.21 Å for regular six-coordinate Ce(IV). It is also considerably less than that reported for the average U−O distance (2.24 Å) in the structure of cubic UP_2O_7 analyzed using a split site model[31] for disorder in the P−O−P oxygen even though the ionic radii for six coordinate U(IV) and Ce(IV) are similar (103 and 101 pm, respectively).[32] The observed short Ce−O distances may be a consequence of considerable disorder in the oxygen bonded to cerium leading to an average position that is significantly closer to the cerium than the instantaneous oxygen positions. The anisotropic nature of the ADPs for this oxygen is consistent with this proposal.

The variable-temperature laboratory X-ray diffraction data indicated an effective linear CTE of $\sim 6.5 \times 10^{-6}$ K^{-1} between room temperature and 115 °C (see Figure 6), and the variable-temperature synchrotron data at −123 °C (150 K) and room temperature (see Table 1) suggested an effective linear CTE of $\sim 14 \times 10^{-6}$ K^{-1} in this temperature range. The synchrotron data also indicated that the thermal expansion of CeP_2O_7 flattens out on cooling below −123 °C (150 K) (see Table 1). Positive thermal expansion is displayed by many $M^{IV}P_2O_7$ phases at low temperatures. Above the transition to cubic symmetry, the linear CTE flattens out and becomes negative at greater than ∼400 °C. This behavior is similar to that seen for ZrV_2O_7.[29] Negative thermal expansion has also been observed at high temperature in the large lattice constant pyrophosphates UP_2O_7 and ThP_2O_7.[7,33]

The high-pressure diffraction measurements provide evidence for two phase transitions on compression at ∼0.65 GPa and ∼5 GPa. The phase existing between these two pressures is quite soft, with a bulk modulus of ∼18 GPa. Prior high-pressure studies of MX_2O_7 materials have also uncovered some low-pressure phase transitions and soft phases at low pressure. For example, cubic ZrV_2O_7 transforms to a pseudotetragonal structure between 1.38 and 1.58 GPa[34] and HfV_2O_7 transforms at around 3.7 ± 0.3 GPa to an undetermined structure,[35] although ZrP_2O_7 and TiP_2O_7 exhibit no pressure-induced phase changes at ambient temperature.[34] TiP_2O_7 and ZrP_2O_7 have been reported to have bulk moduli (B_0) of 42(3) and 39(1) GPa, respectively, somewhat higher than that seen for CeP_2O_7, but α- and β-ZrV_2O_7 (cubic and pseudotetragonal, respectively) and HfV_2O_7 have bulk moduli (B_0) very similar to that seen for CeP_2O_7 at low pressure: 17.0(7), 21(1),[34] and 12.8(4) GPa, respectively.[35]

Acknowledgment. A.P.W. is grateful for support under National Science Foundation Grants DMR-0203342 and DMR-0605671. Some of the high temperature XRD data were collected at the Diffraction User Center, Oak Ridge National Laboratory, sponsored by the Assistant Secretary for Energy Efficiency and Renewable Energy, Vehicle Technologies Program, as part of the High Temperature Materials Laboratory User Program, Oak Ridge National Laboratory, managed by UT-Battelle, LLC, for the U.S. Department of Energy under contract DE-AC05-00OR22725. Ambient pressure synchrotron X-ray measurements were performed at Sector 32, Sector 1, and Sector 11 of the Advanced Photon Source. Use of the Advanced Photon Source was supported by the U.S. Department of Energy, Office of Science, Office of Basic Energy Sciences, under Contract No. DE-AC02-06CH11357. High-pressure diffraction measurements were conducted at the Cornell High Energy Synchrotron Source (CHESS), which is supported by the National Science Foundation and the National Institutes of Health/National Institute of General Medical Sciences under award DMR-0225180.

Supporting Information Available: Tables showing the pseudocubic lattice constant for CeP_2O_7 as a function of both temperature at ambient pressure and pressure at ambient temperature (PDF). This material is available free of charge via the Internet at http://pubs.acs.org.

CM702338H

(29) Korthuis, V.; Khosrovani, N.; Sleight, A. W.; Roberts, N.; Dupree, R.; Warren, W. W. *Chem. Mater.* **1995**, *7*, 412–417.
(30) Roulhac, P. L.; Palenik, G. J. *Inorg. Chem.* **2003**, *42*, 118–121.
(31) Cabeza, A.; Aranda, M. A. G.; Cantero, F. M.; Lozano, D.; Martinez-Lara, M.; Bruque, S. *J. Solid State Chem.* **1996**, *12*, 181–189.
(32) Shannon, R. D. *Acta Crystallogr., Sect. A* **1976**, *32*, 751–767.
(33) Kirchner, H. P.; Merz, K. M.; Brown, W. R. *J. Am. Ceram. Soc.* **1963**, *46*, 137–141.
(34) Carlson, S.; Krogh Andersen, A. M. *J. Appl. Crystallogr.* **2001**, *34*, 7–12.
(35) Hemamala, U. L. C.; El-Ghussein, F.; Goedken, A. M.; Chen, B.; Leroux, C.; Kruger, M. B. *Phys. Rev. B* **2004**, *70*, 214114.